

表面强化技术

基于残余应力分布优化的 TBM 滚刀刀圈 激光熔覆涂层制备工艺研究

崔少杰^{1a,1b}, 王好平^{1a,1b}, 莫继良^{1a,1b}, 蒙树立³, 段文军^{1a,2}, 冯鉴^{1b}

(1.西南交通大学 a.盾构/TBM 装备摩擦学设计实验室 b.机械工程学院, 成都 610031;

2.中铁工程服务有限公司, 成都 610083;

3.中德云岭(四川)工具制造有限责任公司, 成都 611936)

摘要: **目的** 为改善 TBM (全断面隧道掘进机) 涂层刀圈残余应力分布, 针对刀圈涂层制备过程中的激光扫描路径开展研究, 以优化刀圈涂层及涂层/基材界面的残余应力分布。**方法** 使用 MSC. Marc 2016 软件建立了刀圈涂层制备的三维完全热机耦合模型, 通过试验验证了模型的准确性, 并针对激光熔覆过程中扫描顺序、扫描方向和扫描终点夹角等 3 个工艺变量开展了应力场分析研究。**结果** 刀圈表面近涂层区周向/径向残余应力数值计算结果分布趋势与试验基本一致, 且在涂层与基材结合的界面处, 残余应力梯度达到最大, 当激光扫描方向为安装孔到刃顶时, 涂层刀圈残余应力的不合理分布得到了明显改善且应力最值显著降低, 其中基材部分残余应力最高降低 35 MPa, 而调整扫描顺序和扫描终点夹角未能有效改善刀圈残余应力的分布及应力最值。**结论** 通过合理设计熔覆过程中的扫描路线, 可以有效改善刀圈涂层的残余应力分布并降低残余应力最值, 对延长 TBM 涂层刀圈服役寿命具有重要的指导意义。

关键词: TBM 滚刀刀圈; 激光熔覆涂层; 数值仿真; 工艺优化; 残余应力分布

中图分类号: V261.8 **文献标识码:** A **文章编号:** 1001-3660(2023)08-0413-11

DOI: 10.16490/j.cnki.issn.1001-3660.2023.08.037

Preparation of Laser Cladding Coating for TBM Cutter Ring Based on Optimization of Residual Stress Distribution

CUI Shao-jie^{1a,1b}, WANG Hao-ping^{1a,1b}, MO Ji-liang^{1a,1b}, MENG Shu-li³, DUAN Wen-jun^{1a,2}, FENG Jian^{1b}

(1. a. Tribological Design Laboratory of Shield/TBM Equipment, b. School of Mechanical Engineering, Southwest Jiaotong University, Chengdu 610031, China; 2. China Railway Engineering Services Co., Ltd., Chengdu 610083, China;

3. Zongtech Genting (Sichuan) Tool Manufacturing Co., Ltd., Chengdu 611936, china)

收稿日期: 2022-06-17; 修订日期: 2023-02-08

Received: 2022-06-17; Revised: 2023-02-08

基金项目: 国家自然科学基金 (U22A20181、52005419); 四川省科技重点研发项目 (21ZDYF3658)

Fund: The National Natural Science Foundation of China (U22A20181, 52005419); Key Research and Development Project of Sichuan Province (21ZDYF3658)

作者简介: 崔少杰 (1998—), 男, 硕士研究生, 主要研究方向为表面设计及制造。

Biography: CUI Shao-jie (1998-), Male, Postgraduate, Research focus: surface design and manufacturing.

通讯作者: 莫继良 (1982—), 男, 博士, 研究员, 主要研究方向为材料摩擦学及振动噪声。

Corresponding author: MO Ji-liang (1982-), Male, Doctor, Researcher, Research focus: material tribology and vibration noise.

引文格式: 崔少杰, 王好平, 莫继良, 等. 基于残余应力分布优化的 TBM 滚刀刀圈激光熔覆涂层制备工艺研究[J]. 表面技术, 2023, 52(8): 413-423.

CUI Shao-jie, WANG Hao-ping, MO Ji-liang, et al. Preparation of Laser Cladding Coating for TBM Cutter Ring Based on Optimization of Residual Stress Distribution[J]. Surface Technology, 2023, 52(8): 413-423.

ABSTRACT: Metal-matrix ceramic coating can be prepared on the surface of TBM (Tunnel Boring Machine) cutter ring by laser cladding technology to improve the wear resistance, but the residual stress distribution of cutter ring significantly changes in the preparing process. The unreasonable distribution of residual stress of coating may cause low cycle fatigue fracture of cutter ring in service. In this study, the influence of scanning path on stress distribution and maximum/minimum value of stress is studied during the process of coating preparation to decrease the failure risk of TBM coated cutter ring, which will provide theoretical guidance for optimizing the residual stress distribution of coated cutter ring.

A 3D fully thermo-mechanical coupling model of coated cutter ring is established based on the practical laser cladding process (the scanning sequence is "cutter edge \rightarrow cutter edge \rightarrow blade", the scanning direction is from blade to mounting hole and the angle between scanning end points is 120°) of coated TBM cutter ring by MSC. Marc 2016. The radial and hoop residual stress at eight points on the coated cutter ring is measured by X-ray residual stress tester. Compared to the simulation results, it is indicating that the distribution of hoop and radial residual stress near the coated region on the surface of cutter ring by numerical simulation are basically consistent with the experimental results. Moreover, the average residual stress in coating region is 2-3 times higher than that in substrate. The residual stress gradient is the largest at the interface between the coating and substrate. To explore the influence of process variables (scanning sequence, scanning direction and angle between scanning end points) on residual stress distribution of coated cutter ring in laser cladding process, four optimization schemes are designed based on the practical process. Note that these four schemes only change one of process variables compared with the practical process.

In summary, according to the numerical simulation results, the unreasonable distribution of residual stress on the coating surface and the substrate significantly improves by adopting reasonable scanning path. The maximum value of stress obviously decreases when the scanning direction is from the mounting hole to the cutter blade. Especially, the maximum value of residual stress of the substrate decreases by 35 MPa. When the scanning sequence is "blade \rightarrow cutter edge \rightarrow cutter edge", the residual stress distribution of the substrate fails to be improved compared with the practical scheme (cutter edge \rightarrow cutter edge \rightarrow blade), but the residual stress in the coated region of cutter edge decreases significantly. However, when the angle between the scanning end points is adjusted to $0^\circ/90^\circ$, the residual stress distribution of the coated cutter ring has no significant change compared with the practical scheme (120°). Especially, the residual stress of the substrate increases obviously when the angle is 0° . Therefore, the residual stress distribution of coated cutter ring can be improved effectively by reasonably designing the scanning path in the laser cladding process, which has important guiding significance to prolong the service life of TBM coated cutter ring

KEY WORDS: TBM cutter ring; laser cladding coating; numerical simulation; process optimization; distribution of residual stress

TBM 因其开挖效率高、安全性好等特点,近年来在隧道建设工程中得到大力推广^[1]。滚刀作为 TBM 的核心部件^[2],在掘进过程中滚刀刀圈直接承受来自岩石的冲击、剪切及挤压等多重荷载,导致刀圈与岩石之间发生剧烈摩擦磨损(如冲击磨损、黏着磨损和磨粒磨损等)^[3],极易使滚刀刀圈表面发生严重损伤甚至失效行为^[4](如犁沟、剥落和压溃等)。激光熔覆技术^[5]因其粉末选择灵活、效率高、耐磨性提升明显且涂层与基材之间呈良好冶金结合等突出特点,可有效提升滚刀表面耐磨性。国内外关于激光熔覆技术在 TBM 滚刀刀圈上的应用研究已获得初步进展,如:Hu 等^[6]采用激光熔覆技术在刀圈(H13 钢)表面制备了 $\text{Ni}_3\text{Ta-TaC}$ 新型涂层并研究了 TiC 粉末对该涂层性能的影响,研究结果表明 TiC 可明显抑制 Ni_3Ta 金属间化合物的形成,有效降低了涂层的裂纹敏感性;Agrawal 等^[7]在滚刀刀圈小样表面制备了纳米 WC 涂层,在进行硬度与摩擦学试验后发现涂层硬度与磨损

量呈负相关关系,同时涂层抗磨损能力比基材提高了 2~3 倍。综上,目前关于 TBM 滚刀刀圈涂层的研究主要关注涂层材料配比,而制备工艺对刀圈涂层残余应力分布影响的报道较少。

大量研究表明,涂层的制备在关注其抗磨损、耐腐蚀等性能的同时,合理的残余应力分布尤为重要,过高的残余应力或不合理的分布,可能会导致工件在服役过程中产生低周疲劳裂纹甚至发生断裂失效行为^[8-9]。Zhu 等^[10]通过纳米压痕法测取了铁基涂层全厚度的残余应力,结果表明在涂层/基材结合区域残余应力达到最大值 700 MPa,接近基材屈服极限,此区域易成为疲劳裂纹发生点。Hutasoit 等^[11]在 AISI 4130 钢表面分别制备了 Stellite 6 和 Deloro 40G 2 种涂层,并进行了旋转弯曲疲劳试验,结果发现前者涂层区域残余应力水平明显低于后者,但疲劳寿命为后者的 1.5~2 倍,表明较高残余应力水平会减短涂层疲劳寿命。Farahmand 等^[12]通过数值仿真研究了扫描速

度对涂层应力、应变的影响,发现具有较高残余应力的涂层在循环载荷下发生断裂失效的概率明显较高。因此,采用激光熔覆工艺增强刀圈耐磨性时,优化涂层残余应力分布并降低应力最大值是极为重要的。

本文使用 MSC. Marc 2016 软件建立了刀圈涂层制备的三维完全热机耦合模型,利用生死单元法及自主开发的子程序实现了涂层单元的逐步添加及扫描路径的合理规划,再现了涂层熔覆全过程并通过试验验证了模型的准确性,探讨了各工艺变量(扫描顺序、扫描方向及扫描终点间夹角)对涂层及近涂层区基材残余应力的影响,力求通过数值仿真技术探明更优的刀圈涂层激光熔覆制备工艺方案,为生产残余应力合理分布的长寿命全尺寸涂层刀圈提供理论指导。

1 模型建立及试验验证

1.1 基本假设

在对刀圈进行激光熔覆时,激光束与涂层粉末、基材等之间存在复杂的物理化学反应,且由于本文主要关注激光工艺对熔覆试样应力场的影响,所以在进行数值仿真之前建立一些基本的假设是必要的:①忽略刀圈基材初始应力^[13];②涂层和基材材料均各向同性;③出于对计算量的考虑,不计算熔覆过程中的相变应力;④忽略熔覆过程中熔池流动性的影响。

1.2 理论模型及边界条件

1.2.1 热源模型

如图 1 所示,熔覆过程中热源模型采用高斯面热源^[14],其可较好地描述热流密度在工件表面上的分布,数学表达式如式(1)所示。

$$q_s(x, y, z) = \frac{nQ_s}{\pi r^2} \exp\left\{-\frac{n[(x_1 - x_0)^2 + (y_1 - y_0)^2 + (z_1 - z_0)^2]}{r^2}\right\} \quad (1)$$

式中: (x_0, y_0, z_0) 为热源中心坐标, (x_1, y_1, z_1) 为任一节点坐标, $q_s(x, y, z)$ 为该点功率密度, n 为热流集中系数, Q_s 为面热源功率, r 为面热源作用半径。

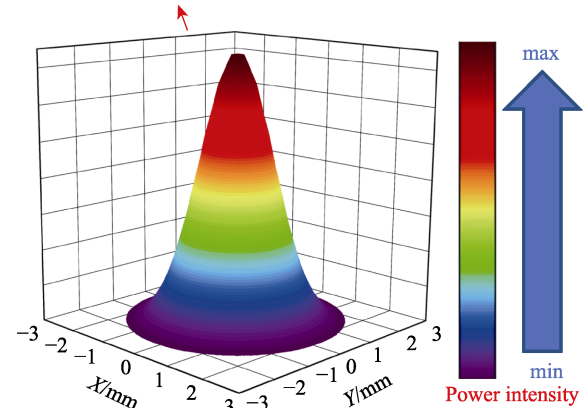


图 1 高斯热源模型

Fig.1 Model of Gaussian heating source

其中 $Q_s=3\ 000\ \text{W}$, $n=0.12$, $r=2\ \text{mm}$, $\pi=3.14$ 。

1.2.2 边界条件及初始条件

选择 TBM 刀盘上常用的弧刀型刀圈作为研究对象,刀圈基本尺寸及边界条件设置如图 2a 所示。其中,涂层(单层)厚度为 2 mm,刃侧涂层宽度为 30 mm,刃顶涂层半径为 13 mm,且为防止刀圈发生刚性位移,将刀圈 2 个端面各自由度进行全约束。模型选用八节点六面体单元,且经过试验验证后发现(如图 2b 所示,横坐标为单元数量,纵坐标为模型计算完成后 A、B 节点等效应力, A、B 两点如图 2a 所示),当单元数量达到 240 000 时,数值仿真结果趋于稳定。因此,基于计算效率及精度的平衡考虑,本文设置模型单元数量为 240 000 (单元尺寸为 1 mm)。

由于涂层与基材极大的热物性参数差别以及激光熔覆过程中急速加热及快速冷却的影响,极易使刀圈产生巨大的热应力。为减小涂层制备后的残余应力,熔覆前将刀圈预热至 200 °C^[15],即在开始计算前设定每一个节点的初始温度为 200 °C,且设定环境温度为 20 °C,热交换系数为 40 W/(m²·°C),同时熔覆过程中的热平衡方程为:

$$\rho c \frac{\partial T}{\partial t} = Q + \frac{\partial}{\partial x} \left(k \frac{\partial T}{\partial x} \right) + \frac{\partial}{\partial y} \left(k \frac{\partial T}{\partial y} \right) + \frac{\partial}{\partial z} \left(k \frac{\partial T}{\partial z} \right) \quad (2)$$

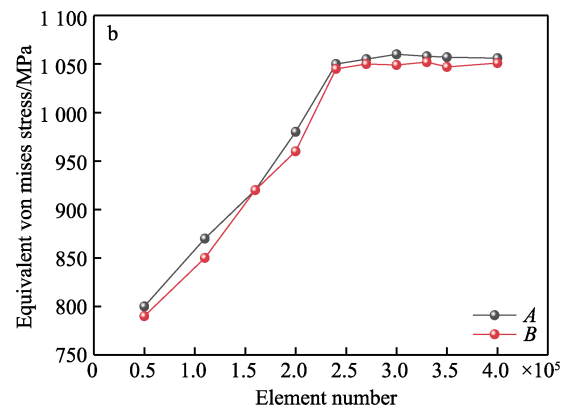
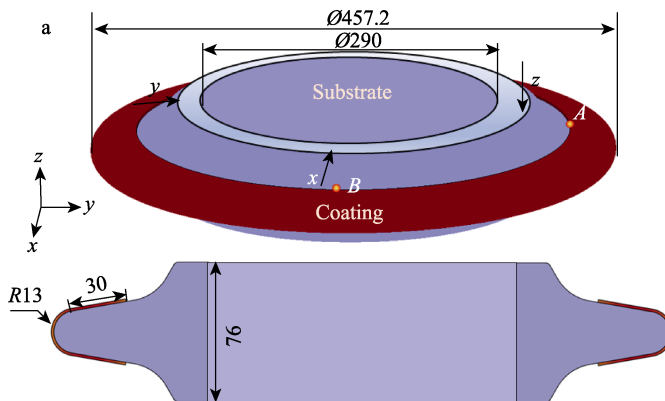


图 2 位移边界条件(a),单元数量验证(b)

Fig.2 Boundary condition (a); Element number verification (b)

式中: ρ 为材料密度, c 为比热容, T 为温度, t 为材料与热源相互作用时间, k 为导热系数, Q 为单位体积产生的热量。

1.2.3 生死单元法及扫描路线

如图3所示,为再现熔覆层“增材”过程,本文采用生死单元法在仿真中实现熔覆层粉末不断被“添加—加热—熔化—冷却—凝固”的过程。基于 MSC. Marc 2016 子程序 uactive 在熔覆开始前利用单元号将所有粉末单元“杀死”,并在熔覆开始即第一个增量步开始时,“复活”以热源中心为圆心、光斑直径为直径的球形范围内的涂层单元,通过子程序使单元“复活”与熔覆过程相配合。

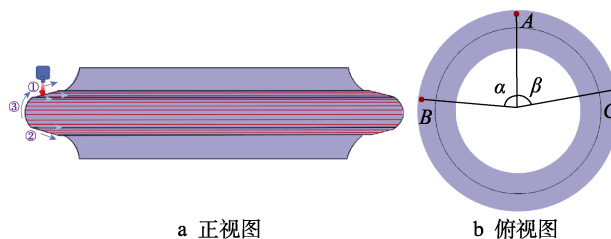


图3 生死单元法原理图

Fig.3 Schematic diagram of birth and death element method

通过 MSC. Marc 2016 子程序 flux 设定了仿真过程中的扫描路线和热源密度。热源在前文已经说明此处不再赘述。对于扫描路线,由于刀圈刃顶和刃侧曲面分别为圆锥面和球面,如图4所示。通过坐标转换的方法计算得出了热源中心在这两种曲面上的螺旋扫描路径(锥面螺旋线、球面螺旋线),且扫描顺序

为刃侧—刃顶—刃侧,刃侧扫描方向为自刃顶向安装孔,扫描终点 A 、 B 、 C (A 、 B 为刃侧扫描终点, C 为刃顶扫描终点) 之间的夹角 $\alpha=\beta=120^\circ$, 与实际生产工艺保持一致。



a 正视图

b 俯视图

图4 扫描方案示意图

Fig.4 Schematic diagram of scanning scheme:

a) front view; b) vertical view

1.2.4 基材及合金粉末的热物性参数

由于 WC 具有高硬度、高耐磨性、高熔点等特性且不易与其他金属发生反应,而金属基的添加可以提高熔覆层的韧性,防止其脆性过高而发生开裂失效^[17-18]。因此,在本研究工作中,熔覆层制备选用 Ni 基 WC 粉末 (WC 粒径: 45~75 μm 约 15%, 75~125 μm 约 60%, 125~150 μm 约 25%; Ni 基粉末粒径: 53~58 μm 约 2.2%, 45~53 μm 约占 97.8%), 球形 WC 粉末含量约占 60%, Ni 基粉末含量约占 40%。同时,基材选用 TBM 刀圈常用材料 H13 钢^[15]。基材与涂层热物性参数如图5所示,其中涂层热物性参数根据线

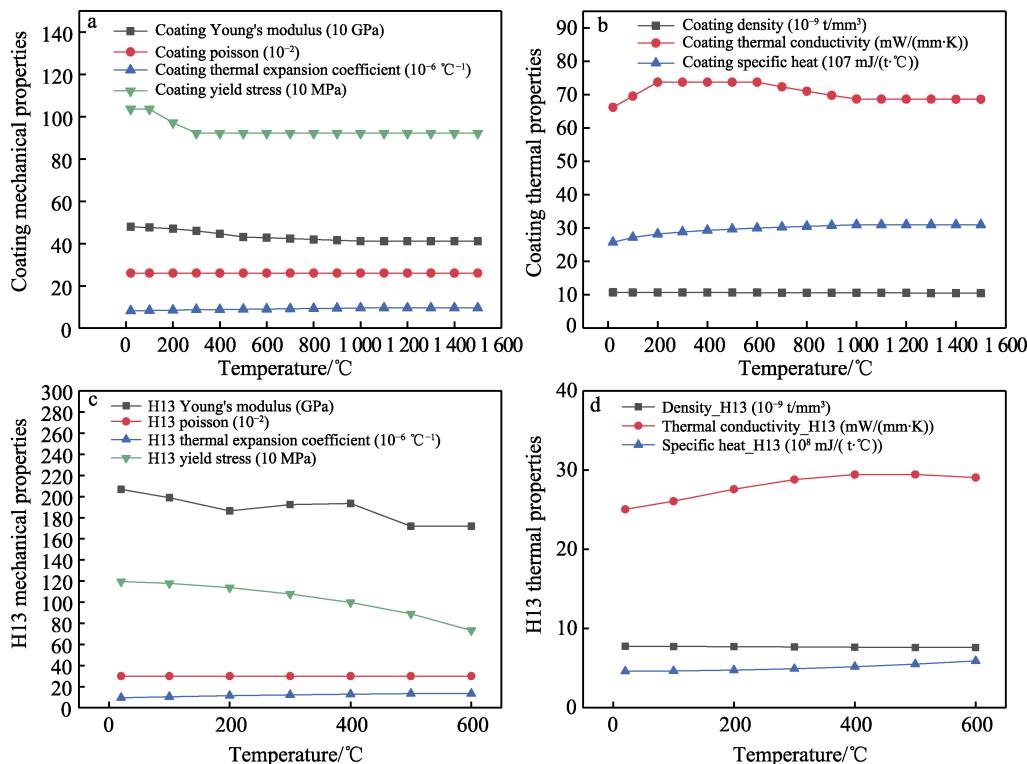


图5 涂层、H13 热物性参数: (a、b) 涂层; (c、d) H13

Fig.5 Thermo-mechanical properties of coating and H13: a, b) coating; c, d) H13

性混合准则^[19]计算得出, 具体公式为:

$$M_c = \frac{M_i B_i + M_o B_o}{B_i + B_o}$$

(3)

式中: B 代表质量分数, M 代表材料性质 (如密度、热导率、比热容等), 下标 c 、 i 、 o 分别代表涂层、WC、金属基粉末。

1.3 模型验证

1.3.1 涂层制备工艺设计

试验中采用功率为 4 kW 的半导体激光器制备涂层, 激光器具体参数及扫描参数见表 1。如图 6 所示, 熔覆过程中使用高精度机械臂完成扫描路线, 其中扫描顺序为刃侧—刃侧—刃顶, 刃侧扫描方向为自刃顶到安装孔, 扫描终点间夹角 $\alpha=\beta=120^\circ$, 且为降低涂层裂纹出现几率, 熔覆前将刀圈预热至 $200\text{ }^\circ\text{C}$ ^[20]。

1.3.2 模型验证试验

采用 μ -X360n 残余应力测试仪 (如图 7a 所示) 对熔覆完成后的刀圈进行残余应力测量, 其误差小于 $\pm 10\text{ MPa}$, 束光器直径为 1 mm, 靶材为 Cr。试验前使用电子量角器使测量仪器与样品表面所测残余应力方向竖直夹角呈 20° , 水平夹角呈 0° , 且试验中主要测取试样径向和周向残余应力。由于涂层制备完成后其表面较为粗糙, 直接测取其表面应力结果偏差较大。因此, 测量点选择在近涂层区的基材表面上, 且每隔 45° 对测点进行测量, 如图 7b 所示。

数值模型计算完成后, 按照应力测量试验中测量点位置测取了模型中相应 8 个点的径向与周向应力, 并将仿真结果与试验测量结果进行对比。如图 8 所示, 图中以测量点对应角度为横坐标, 以应力值为纵坐标, 发现仿真结果与试验结果趋势吻合良好, 可证

表 1 激光熔覆工艺参数
Tab.1 Process parameters of laser cladding

Laser parameters				Scanning parameters		
Spot diameter/ mm	Wavelength/ μm	Fiber diameter/ μm	Power/ kW	Scanning velocity/ ($\text{mm}\cdot\text{min}^{-1}$)	Overlap ratio (blade)/%	Overlap ratio (edge)/%
4	915	600	3	900	50	25

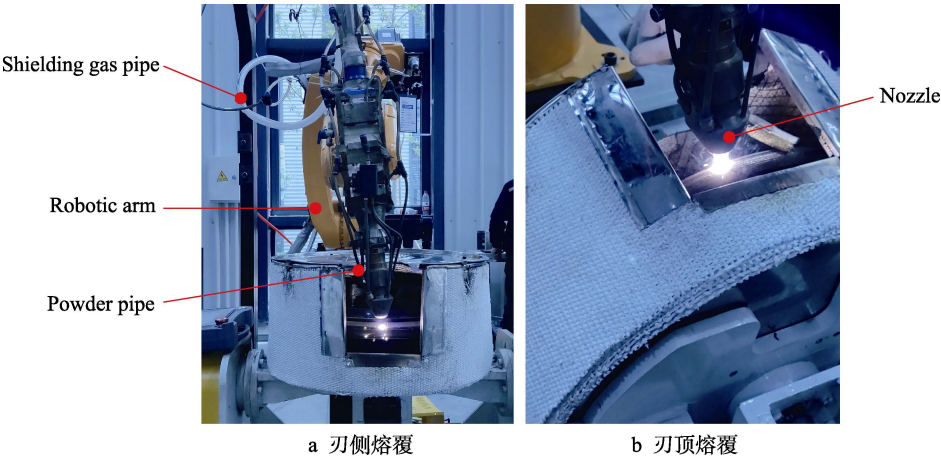


图 6 激光熔覆过程
Fig.6 Process of laser cladding: a) cutter edge; b) cutter blade

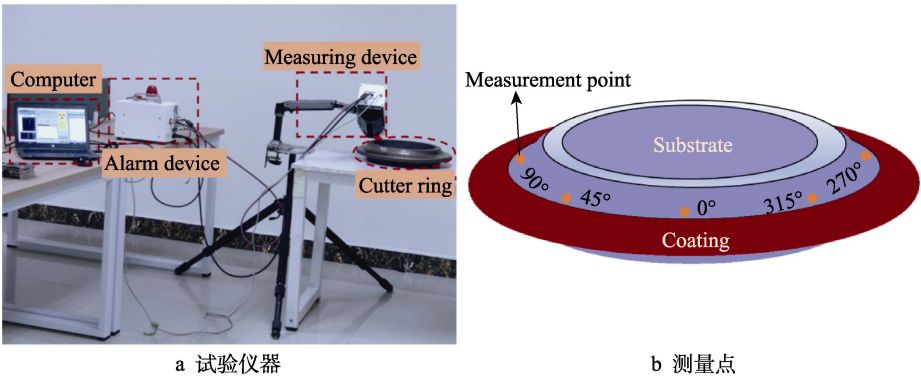


图 7 应力测量试验
Fig.7 Stress measurement experiment: a) experimental instruments; b) measuring point

明模型准确性。但在数值上存在差异,数值上的差异来源可能是没有考虑基材热处理、锻造成形后的残余应力以及在熔覆过程中基材产生的相变应力等^[21]。

根据试验结果可知,按照实际熔覆工艺制备的涂层刀圈残余应力分布极不均匀且应力水平偏高,周向应力曲线波峰波谷之间的差值超过 300 MPa,径向应力曲线波峰波谷之间的差值超过 200 MPa,残余应力分布梯度过大。图 9 展示了 0°和 180°测量点 A 和 B 在熔覆过程中的温度和等效应力历程曲线,总体上

看,两测点的温度和等效应力均随时间延长呈现周期性非稳态变化的特点,其中 B 点先于 A 点受热,致使在熔覆初期 B 点温度高于 A 点。但随熔覆的进行,热累积促使 A 点温度高于 B 点,从而使 B 点的变形量低于 A 点,致使二者的应力出现显著差异。在此残余应力分布状态下,刀圈裂纹敏感性明显升高,作业时极易出现裂纹及非正常磨损^[22-23],对实际熔覆工艺方案进行优化并改善涂层刀圈的应力分布显得十分必要。

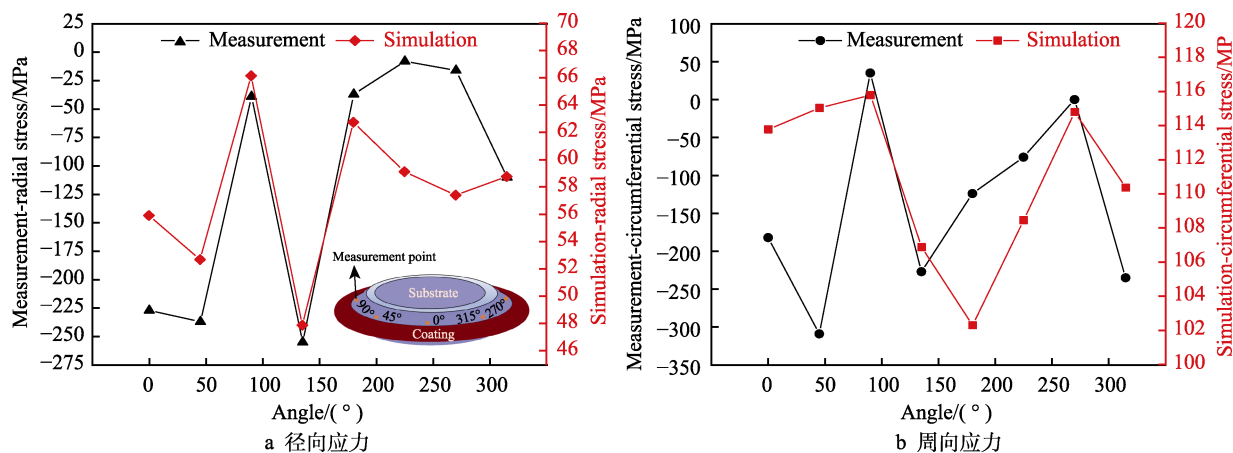


图 8 仿真与试验结果对比图

Fig.8 Result comparison between simulation and experiment: a) radial stress; b) hoop stress

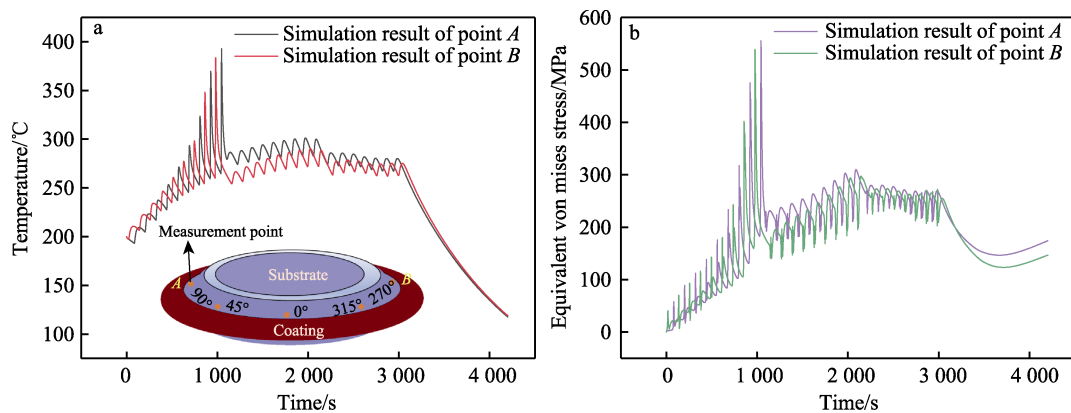


图 9 温度及等效应力历程曲线

Fig.9 Temperature and Mises stress history curve

2 涂层制备数值仿真分析方案

在激光熔覆过程中,若保持比能量一致,扫描顺序(刀侧—刀侧—刀顶或刀顶—刀侧—刀侧)、扫描

方向(自刃顶向安装孔方向还是反向)以及扫描终点间夹角等扫描方式对涂层残余应力的分布影响最大^[24]。本文以上述 3 种工艺变量为基准,在实际熔覆工艺方案基础上设计了 4 种优化方案,并分别对其进行数值仿真,5 种工艺及其命名方案如表 2 所示。实际熔覆工艺方案变

表 2 各工况方案设计

Tab.2 Scheme design of each working condition

No.	Angle between scanning end points	Scanning direction	Scanning sequence
Stp-1	0°	From blade to mounting hole	Cutter edge—cutter edge—blade
Stp-2	90°	From blade to mounting hole	Cutter edge—cutter edge—blade
Stp-3	120°	From blade to mounting hole	Cutter edge—cutter edge—blade
Lcd-1	120°	From mounting hole to blade	Cutter edge—cutter edge—blade
Lco-1	120°	From blade to mounting hole	Blade—cutter edge—cutter edge

量名为 Stp-3, 即: 扫描顺序为刃侧—刃侧—刃顶, 刃侧扫描方向为自刃顶到安装孔, 扫描终点之间夹角为 120° ,

其他 4 种工艺方案均是在实际工艺方案 Stp-3 基础上进行调整且仅改变一种工艺变量。图 10 为熔覆方案简图。

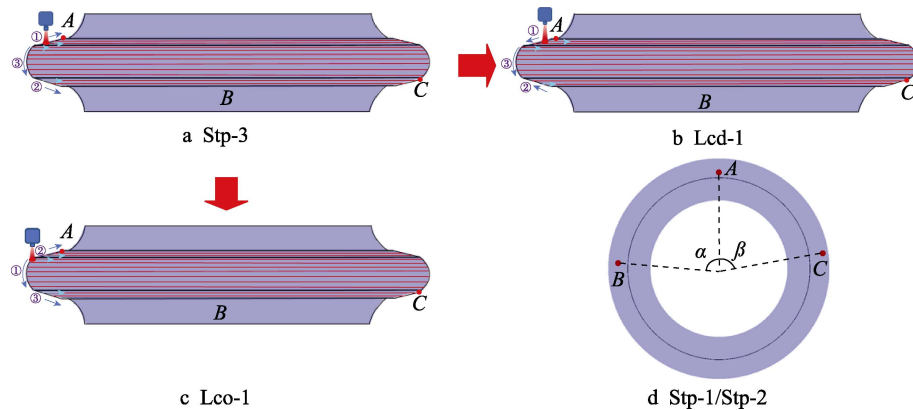


图 10 仿真工艺方案简图

Fig.10 Schematic diagram of simulation process scheme

3 仿真分析结果与讨论

3.1 激光熔覆工艺对基材残余应力分布的影响

熔覆过程中, 刀圈在激光高密度能量束的作用下, 导致在近涂层区的基材残余应力发生突变, 严重影响基材疲劳寿命^[25]。本节基于上述 5 种仿真模型, 每隔 45° 测取了刀圈靠近涂层边缘基材 8 个位置的等效应力, 以探究不同扫描方式对基材的影响程度, 结果如图 11 所示。与 Stp-2、Stp-3 相比, 可看出当扫描终点夹角为 0° (Stp-1) 时, 基材残余应力明显升高, 此时刃侧与刃顶扫描终点在同一平面上, 导致应力集中, 应根据工艺需求选取较大的扫描终点夹角。对比 Stp-3 和 Lco-1 可知, 当扫描顺序为刃顶—刃侧—刃侧时, 与原始工艺相比刀圈基材残余应力的分布几乎一致, 改变扫描顺序并不能有效改善基材残余应力分布。而综合比较 Lcd-1 与其他 4 条曲线, 发现其等效应力波动及均值明显降低, 有利于抑制疲劳裂纹

萌生^[26]。可见将扫描方向改为自安装孔到刃顶后, 此时熔覆路径初始端靠近安装孔, 随着熔覆的进行, 初始熔覆的涂层会被重新加热并发生应力释放^[27], 从而降低了基材区域的残余应力, 相比于其他 4 种工艺方案可以更好地改善基材残余应力的分布。

3.2 激光熔覆工艺对涂层表面残余应力分布的影响

刀圈在不同扫描方式下的等效应力分布情况如图 12 所示。首先通过图 12a—c 可看出, 在 Stp-1、Stp-2、Stp-3 扫描方式下涂层表面残余应力分布几乎一致, 说明改变扫描终点间夹角对涂层残余应力分布的影响很小, 且由于刃顶部分最后熔覆导致涂层表面的残余应力主要集中在刃顶部分, 这与 Farahmand 等^[12]在平板上熔覆得出的结论相一致。将刃侧扫描方向改为自安装孔向刃顶后, 残余应力主要集中在刃侧与刃顶的结合部分, 如图 12d 所示。而当扫描顺序为刃顶—刃侧—刃侧时, 残余应力主要集中在刃侧熔覆的最后几道, 如图 12e 所示。

为准确分析每种扫描方案下刀圈涂层表面的残余应力分布情况, 每隔 90° 截取刀圈的 4 个截面并分别测取每个截面涂层表面节点的等效应力, 如图 13 所示, 横坐标为节点编号, 纵坐标为等效米塞斯应力。首先通过 4 幅曲线图可知, 在不同角度的涂层表面残余应力分布状态大致相同; 其次, Stp-1、Stp-2、Stp-3 曲线几乎重合, 其在刃侧区域波动较大, 在刃顶区域比较平缓但应力值偏大, 可见仅改变扫描终点夹角并不能有效改善涂层表面的残余应力分布; 而比较 Lco-1 和 Stp-3 后发现, 二者残余应力分布状态呈相反趋势, 这与将熔覆顺序改为刃顶—刃侧—刃侧有关, 残余应力主要在刃侧集中; 当改变扫描方向后, 相比于其他 4 条曲线, Lcd-1 整条曲线变得较为平缓, 残余应力分布得到明显改善, 有效降低了涂层表面裂纹敏感性^[28]。

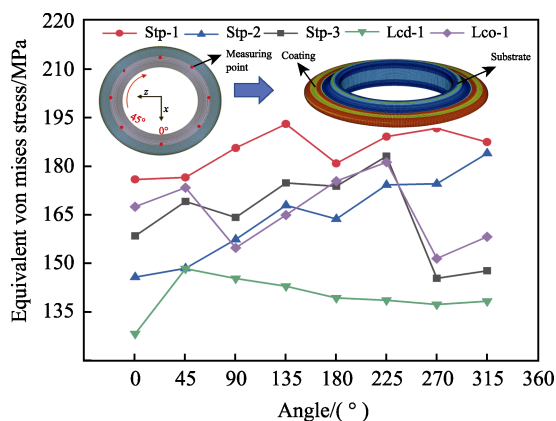


图 11 扫描方式对基材残余应力的影响

Fig.11 Effect of scanning scheme on residual stress of substrate

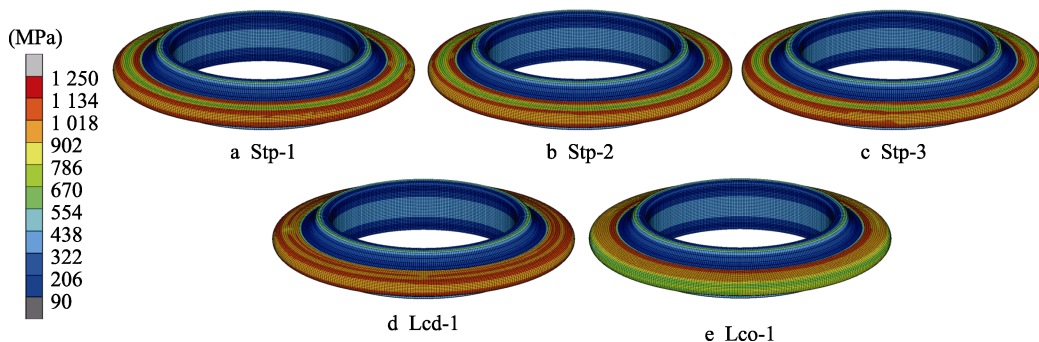


图12 刀圈等效米塞斯应力分布云图

Fig.12 Equivalent Mises stress distribution of cutter ring

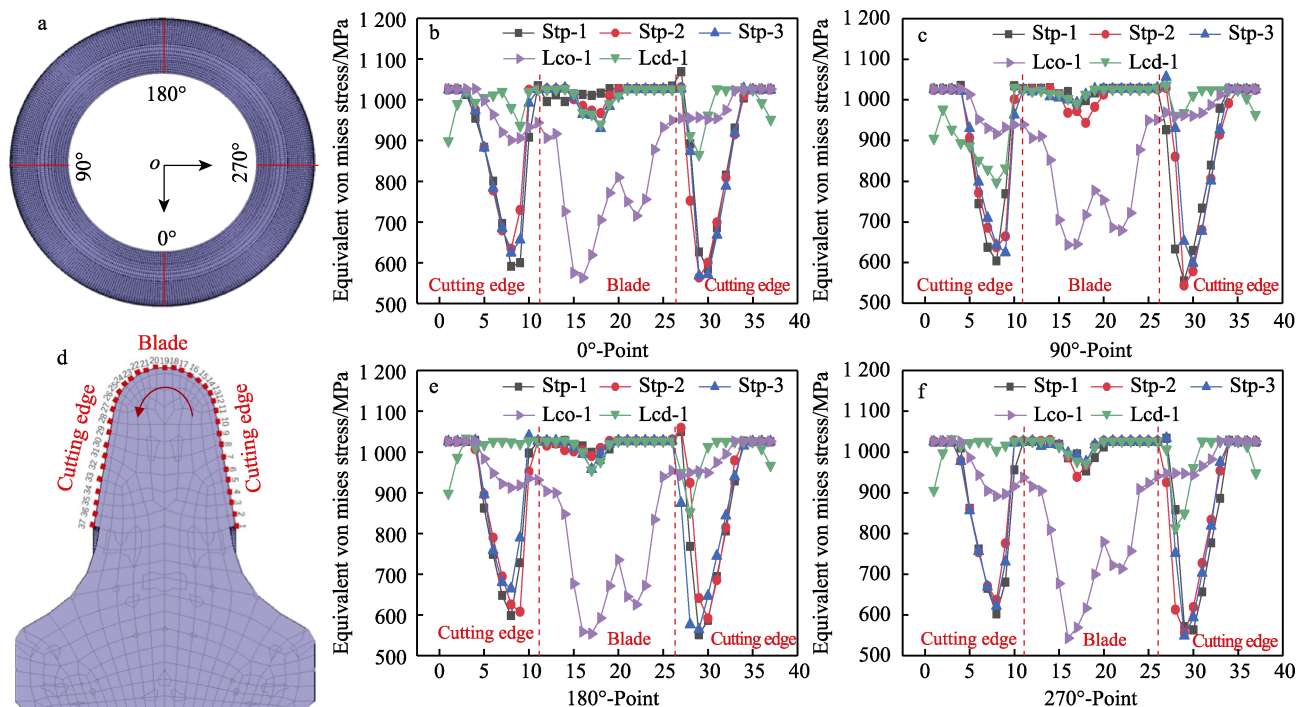


图13 涂层表面等效米塞斯应力分布: (a、d)分析取点示意图; (b) 0°截面; (c) 90°截面; (e) 180°截面; (f) 270°截面

Fig.13 Equivalent Mises stress distribution on coating surface: (a, d) measuring scheme; (b) 0° section; (c) 90° section; (e) 180° section; (f) 270° section

为使仿真结果更加直观,图14统计了图13中各工艺曲线的标准差。结果显示,Lcd-1标准差值远低于其余4条曲线,特别相对于原始工况Stp-3,仅为

其标准差的1/3~1/2,表明其平稳性远优于其余4条曲线,进一步证明了改变扫描方向可有效改善TBM刀具涂层表面的应力分布。

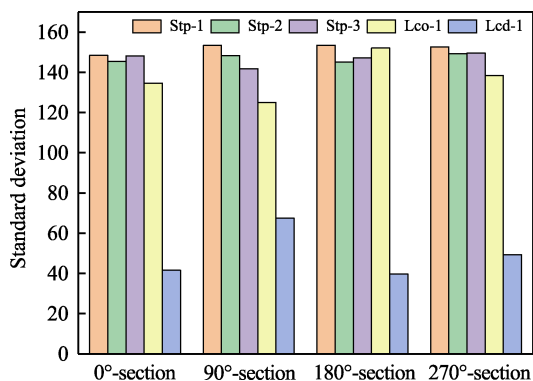


图14 各工艺曲线标准差统计图

Fig.14 Standard deviation chart of each curve

3.3 激光熔覆工艺对刀圈截面残余应力分布的影响

刀圈在服役过程中,内部缺陷的产生主要与刀圈内的残余应力分布相关^[29],本节主要探讨不同扫描方案对涂层刀圈截面残余应力分布的影响。选取刀圈2个位置0°、90°(如图13a所示)的截面,从涂层边缘开始每隔3mm左右测量1次等效应力值,如图15所示(横坐标为与第1个测量点的距离,纵坐标为等效米塞斯应力)。可看到尽管按照不同的扫描方案对刀圈进行熔覆,但它们对刀圈截面残余应力分布的影响效果几乎相同。而由于涂层材料与基材之间热膨胀

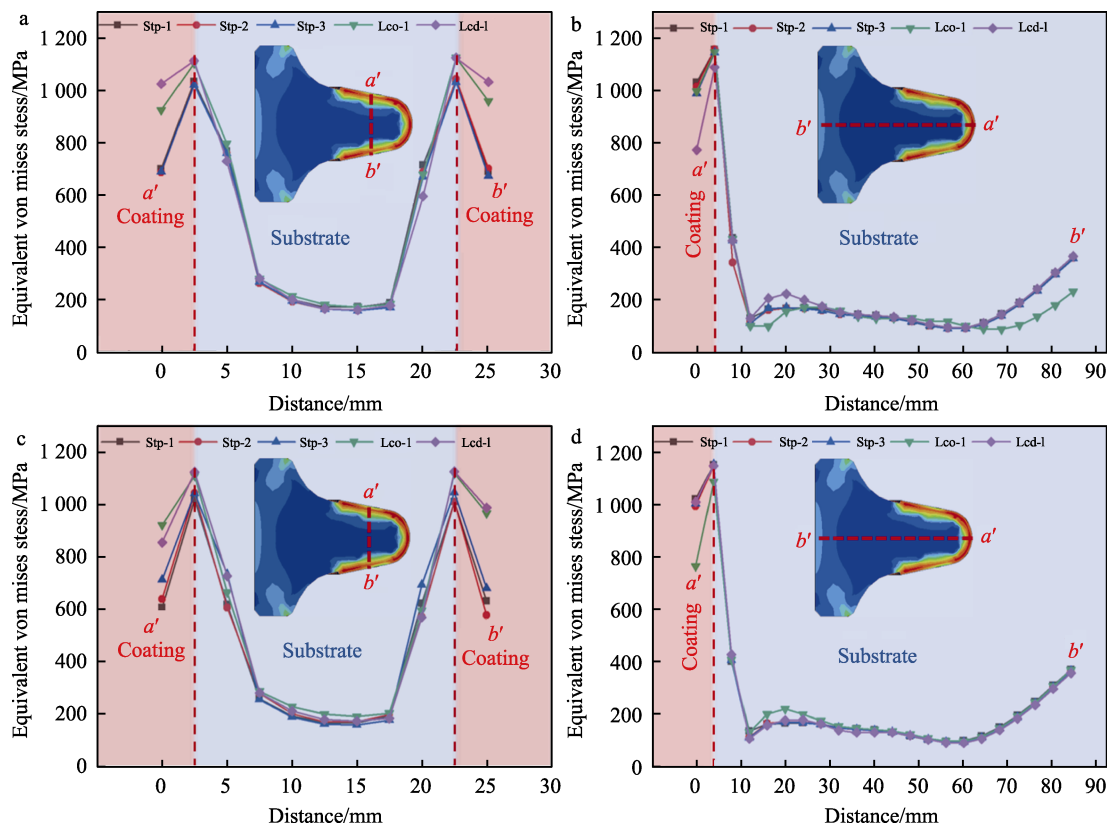


图 15 刀圈内部残余应力分布: (a、b) 0°截面; (c、d) 90°截面
Fig.15 Residual stress distribution in the cutter ring: (a, b) 0°section; (c, d) 90°section

系数存在差异, 导致在对刀圈表面进行熔覆时基材与涂层的热应变速率差距过大, 二者之间相互拉压, 使熔覆后刀圈的残余应力集中在涂层和基材的结合线区域且涂层区域残余应力平均值为基材的 4~5 倍。

4 结论

1) 模型准确性。基于 MSC. Marc 2016 软件建立了 TBM 涂层刀圈的三维热机耦合模型并采用生死单元法及自主开发的子程序再现了涂层制备全过程, 模型表面的径向、周向残余应力分布趋势与试验结果表现出较好的一致性, 证明了模型的准确性。

2) 合理的扫描路线可有效改善涂层刀圈表面残余应力分布。不同扫描终点夹角对涂层刀圈表面残余应力分布的影响效果几乎一致, 无法有效改善涂层刀圈表面残余应力分布; 调整熔覆顺序后, 基材部分残余应力变化不明显, 涂层刃顶部分残余应力明显降低, 但涂层刃侧部分残余应力显著升高, 涂层表面残余应力分布仍不够合理; 扫描方向调整为自安装孔到刃顶后, 基材部分残余应力明显降低, 且刃侧与刃顶涂层残余应力水平相当, 涂层刀圈表面残余应力分布得到明显改善。

3) 改变扫描方向、扫描顺序以及扫描终点间夹角对涂层刀圈截面残余应力分布的影响不明显。当改

变上述 3 种工艺变量时, 三者的影响效果几乎一致且刀圈截面残余应力集中在涂层与基材的结合线区域, 无法有效改善涂层刀圈截面残余应力分布。

参考文献:

- [1] HUO Jun-zhou, SUN Wei, CHEN Jing, et al. Disc Cutters Plane Layout Design of the Full-Face Rock Tunnel Boring Machine (TBM) Based on Different Layout Patterns[J]. Computers & Industrial Engineering, 2011, 61(4): 1209-1225.
- [2] REN Dong-jie, SHEN Shui-long, ARULRAJAH A, et al. Prediction Model of TBM Disc Cutter Wear during Tunneling in Heterogeneous Ground[J]. Rock Mechanics and Rock Engineering, 2018, 51(11): 3599-3611.
- [3] BARZEGARI G, UROMEIHY A, ZHAO Jian. Parametric Study of Soil Abrasivity for Predicting Wear Issue in TBM Tunneling Projects[J]. Tunneling and Underground Space Technology, 2015, 48: 43-57.
- [4] 段文军, 李贞, 王好平, 等. 盾构滚刀材料表面镍基碳化钨涂层摩擦学性能研究[J]. 表面技术, 2021, 50(1): 313-321, 365.

DUAN Wen-jun, LI Zhen, WANG Hao-ping, et al. Tribological Properties of Ni-Based WC Coating Prepared on

- Shield Disc Cutter Material Surface[J]. Surface Technology, 2021, 50(1): 313-321, 365.
- [5] 张津超, 石世宏, 龚燕琪, 等. 激光熔覆技术研究进展[J]. 表面技术, 2020, 49(10): 1-11.
ZHANG Jin-chao, SHI Shi-hong, GONG Yan-qi, et al. Research Progress of Laser Cladding Technology[J]. Surface Technology, 2020, 49(10): 1-11.
- [6] HU Deng-wen, LIU Yan, CHEN Hui, et al. Effect of TiC Addition on the Microstructure and Properties of Ni₃Ta-TaC Reinforced Ni-Based Wear-Resistant Coating[J]. Ceramics International, 2021, 47(16): 23194-23202.
- [7] AGRAWAL A K, CHATTOPADHYAYA S, MURTHY V M S R, et al. A Novel Method of Laser Coating Process on Worn-out Cutter Rings of Tunnel Boring Machine for Eco-Friendly Reuse[J]. Symmetry, 2020, 12(3): 471.
- [8] BARAGETTI S. Fatigue Resistance of Steel and Titanium PVD Coated Spur Gears[J]. International Journal of Fatigue, 2007, 29(9-11): 1893-1903.
- [9] WANG Qian, SHI Jun-miao, ZHANG Li-xia, et al. Impacts of Laser Cladding Residual Stress and Material Properties of Functionally Graded Layers on Titanium Alloy Sheet[J]. Additive Manufacturing, 2020, 35: 101303.
- [10] ZHU Li-na, XU Bin-shi, WANG Hai-dou, et al. Microstructure and Nanoindentation Measurement of Residual Stress in Fe-Based Coating by Laser Cladding[J]. Journal of Materials Science, 2012, 47(5): 2122-2126.
- [11] HUTASOIT N, LUZIN V, BLICBLAU A, et al. Fatigue Life of Laser Clad Hardfacing Alloys on AISI 4130 Steel under Rotary Bending Fatigue Test[J]. International Journal of Fatigue, 2015, 72: 42-52.
- [12] FARAHMAND P, KOVACEVIC R. An Experimental-Numerical Investigation of Heat Distribution and Stress Field in Single- and Multi-Track Laser Cladding by a High-Power Direct Diode Laser[J]. Optics & Laser Technology, 2014, 63: 154-168.
- [13] 于庆增, 龙伟漾, 杨兴亚, 等. 具有不同硬度梯度的热处理工艺对盾构刀圈组织和力学性能的影响[J]. 热加工工艺, 2020, 49(12): 150-152, 156.
YU Qing-zeng, LONG Wei-yang, YANG Xing-ya, et al. Effects of Heat Treatment Process with Different Hardness Gradients on Microstructure and Mechanical Properties of Shield Cutter Ring[J]. Hot Working Technology, 2020, 49(12): 150-152, 156.
- [14] 罗心磊, 刘美红, 黎振华, 等. 不同热源模型对选区激光熔化 18Ni300 温度场计算结果的影响[J]. 中国激光, 2021, 48(14): 52-62.
LUO Xin-lei, LIU Mei-hong, LI Zhen-hua, et al. Effect of Different Heat-Source Models on Calculated Temperature Field of Selective Laser Melted 18Ni300[J]. Chinese Journal of Lasers, 2021, 48(14): 52-62.
- [15] JENDRZEJEWSKI R, SLIWINSKI G, CONDE A, et al. Influence of the Base Preheating on Cracking of the Laser-Cladded Coatings[C]//Proc SPIE 5121, Laser Processing of Advanced Materials and Laser Microtechnologies, 2003, 5121: 356-361.
- [16] YAN Hong, HUA J, SHIVPURI R. Numerical Simulation of Finish Hard Turning for AISI H13 Die Steel[J]. Science and Technology of Advanced Materials, 2005, 6(5): 540-547.
- [17] XIE Hong-xian, SONG Xiao-yan, YIN Fu-xing, et al. Effect of WC/Co Coherency Phase Boundaries on Fracture Toughness of the Nanocrystalline Cemented Carbides[J]. Scientific Reports, 2016, 6: 31047.
- [18] DAVIS J R. ASM Specialty Handbook-Copper and Copper alloys[M]. ASM International Staff, 2001: 510-512.
- [19] WOO Y, HWANG T, OH I, et al. Analysis on Selective Laser Melting of WC-Reinforced H13 Steel Composite Powder by Finite Element Method[J]. Advances in Mechanical Engineering, 2019, 11(1): 168781401882220.
- [20] 王冉, 王玉玲, 姜芙林, 等. 基体预热对激光熔覆制备 Al₂O₃-ZrO₂ 陶瓷涂层裂纹敏感性的影响[J]. 表面技术, 2022, 51(3): 342-352.
WANG Ran, WANG Yu-ling, JIANG Fu-lin, et al. Effect of Substrate Preheating on Crack Sensitivity of Al₂O₃-ZrO₂ Ceramic Coating Prepared by Laser Cladding[J]. Surface Technology, 2022, 51(3): 342-352.
- [21] CHEN Yong, LIU Yan, CHEN Hui, et al. Multi-Scale Residual Stress Prediction for Selective Laser Melting of High Strength Steel Considering Solid-State Phase Transformation[J]. Optics & Laser Technology, 2022, 146: 107578.
- [22] 董世运, 闫晓玲, 徐滨士. 微观组织及残余应力对瑞利波评价激光熔覆层应力的影响[J]. 机械工程学报, 2015, 51(24): 50-56.
DONG Shi-yun, YAN Xiao-ling, XU Bin-shi. Influence of Microstructure and Residual Stress on Surface Stress Measurement of Laser Cladding Layer by Rayleigh Wave[J]. Journal of Mechanical Engineering, 2015, 51(24): 50-56.
- [23] ZHANG Yao-cheng, YANG Li, CHEN Ting-yi, et al. Sensitivity of Liquation Cracking to Deposition Parameters and Residual Stresses in Laser Deposited IN718 Alloy[J]. Journal of Materials Engineering and Performance, 2017, 26(11): 5519-5529.
- [24] REN K, CHEW Y, FUH J Y H, et al. Thermo-Mechanical Analyses for Optimized Path Planning in Laser Aided Additive Manufacturing Processes[J]. Materials & Design, 2019, 162: 80-93.
- [25] 李广琪, 王丽芳, 朱刚贤, 等. 扫描方式对中空环形激光熔覆层残余应力及基板变形的影响研究[J]. 表面技

- 术, 2021, 50(3): 158-170.
- LI Guang-qi, WANG Li-fang, ZHU Gang-xian, et al. Influence of Scanning Patterns on Residual Stress of Cladding Layer and Substrate Deformation Produced by Hollow-Ring Laser Cladding[J]. Surface Technology, 2021, 50(3): 158-170.
- [26] CHEW Y, PANG J H L, BI Gui-jun, et al. Thermo-Mechanical Model for Simulating Laser Cladding Induced Residual Stresses with Single and Multiple Clad Beads[J]. Journal of Materials Processing Technology, 2015, 224: 89-101.
- [27] KARPENKO O, OTERKUS S, OTERKUS E. Investigating the Influence of Residual Stresses on Fatigue Crack Growth for Additively Manufactured Titanium Alloy Ti6Al4V by Using Peridynamics[J]. International Journal of Fatigue, 2022, 155: 106624.
- [28] SUN Wen-bo, MA Yu e, LI Pei-yao, et al. Residual Stress and Long Fatigue Crack Growth Behaviour of Laser Powder Bed Fused Ti6Al4V: Role of Build Direction[J]. International Journal of Fatigue, 2022, 160: 106850.
- [29] LEE Chang-min, PARK H, YOO J, et al. Residual Stress and Crack Initiation in Laser Clad Composite Layer with Co-Based Alloy and WC+NiCr[J]. Applied Surface Science, 2015, 345: 286-294.

责任编辑: 万长清

(上接第 386 页)

- [27] EL-BAHY S M, ARSHAD J, MUNIR S, et al. Improved Photocatalytic Performance of a New Silver Doped BiSbO₄ Photocatalyst[J]. Ceramics International, 2022, 48(16): 23914-23920.
- [28] BERTI G. Background and Bragg Scattering Component Separation in Powders via the XRD Technique[J]. Materials Science Forum, 1993, 136: 83-88.
- [29] GAO Y, HE H W, TAN W Y, et al. One-step Potentiostatic Electrodeposition of Ni-Se-Mo Film on Ni Foam for Alkaline Hydrogen Evolution Reaction[J]. International Journal of Hydrogen Energy, 2020, 45(11): 6015-6023.
- [30] WU Yi-hui, HE Han-wei. Electrodeposited Nickel-Iron-Carbon-Molybdenum Film as Efficient Bifunctional Electrocatalyst for Overall Water Splitting in Alkaline Solution[J]. International Journal of Hydrogen Energy, 2019, 44(3): 1336-1344.
- [31] SEQUEIRA C A C, SANTOS D M F, BRITO P S D. Electrocatalytic Activity of Simple and Modified Fe-P Electrodeposits for Hydrogen Evolution from Alkaline Media[J]. Energy, 2011, 36(2): 847-853.
- [32] WANG Ying, YAO Yao, CHEN Yu, et al. Pt₃Ni@C Composite Material Designed and Prepared Based on Volcanic Catalytic Curve and Its High-Performance Static Lithium Polysulfide Semiliquid Battery[J]. Nanomaterials, 2021, 11(12): 3416.
- [33] 吁艳林. 密度泛函理论计算在 Ni 基析氢电极研究中的应用[D]. 北京: 北京有色金属研究总院, 2017: 15-16.
- YU Yan-lin. Application of Density Functional Theory Calculation in the Study of Ni-Based Hydrogen Evolution Electrode[D]. Beijing: 北京有色金属研究总院, 2017: 15-16.
- [34] NOERSKOV J K, BLIGAARD T, LOGADOTTIR A, et al. Trends in the Exchange Current for Hydrogen Evolution[J]. Journal of the Electrochemical Society, 2005, 152(3): 23-26.
- [35] ZHOU Yong-fang, LIN Ting-ting, LUO Xuan-li, et al. Mechanistic Study on Nickel-Molybdenum Based Electrocatalysts for the Hydrogen Evolution Reaction[J]. Journal of Catalysis, 2020, 388: 122-129.
- [36] WANG G W, LI W Z, HUANG B, et al. Exploring the Composition-Activity Relation of Ni-Cu Binary Alloy Electrocatalysts for Hydrogen Oxidation Reaction in Alkaline Media[J]. ACS Applied Energy Materials, 2019, 2(5): 3160-3165.

责任编辑: 彭颀